

Argonne, April 4 - 7, 2006

## Three-body decay of nuclear resonances

A.S. Jensen<sup>1</sup>, D.V.Fedorov<sup>1</sup>, E. Garrido<sup>2</sup> H. Fynbo<sup>1</sup>

<sup>1</sup>IFA, University of Aarhus, DK-8000 Aarhus C

<sup>2</sup>Instituto de Estructura de la Materia, CSIC, E-28006 Madrid

### **CONTENT**

1. Theoretical formulation
2. Short-range interaction
3. Two large scattering lengths
4. Short-range plus Coulomb interaction
5. Isospin mixing
6. Summary and conclusions

## Theoretical formulation:

Coordinates:  $(\mathbf{x}, \mathbf{y})$  are mass scaled Jacobi coordinates

$\mathbf{r}_{ij}$  is the vector connecting particle  $i$  and  $j$

$$x^2 = r_{ik}^2 \frac{m_i m_k}{m(m_i + m_k)}$$

$$y^2 = r_{j,ik}^2 \frac{m_j(m_i + m_k)}{m(m_i + m_k + m_j)}$$

$$\rho^2 = x^2 + y^2 = \frac{1}{m(m_i + m_k + m_j)} \sum_{i < j} m_i m_j r_{ij}^2$$

$\Omega = \{\Omega_x, \Omega_y, \alpha\}$ , i.e. directions of  $(\mathbf{x}, \mathbf{y})$  and  $\tan \alpha = \frac{x}{y}$

Complex scaling:  $\rho \rightarrow \rho \exp(i\theta)$

Adiabatic hyperspherical expansion:

Choose interactions and solve Faddeev equations for each  $\rho$

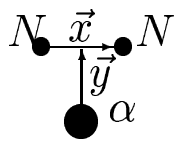
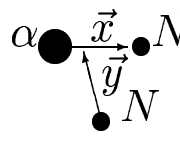
Compute angular eigenvalues  $\lambda_n$  and eigenfunctions  $\{\Phi_n(\rho, \Omega)\}$

The three-body bound state or resonance wave function  $\Psi$  is:

$$\begin{aligned} \Psi(\mathbf{x}, \mathbf{y}) &= \sum_n f_n(\rho) \Phi_n(\rho, \Omega) \\ &= \sum_n f_n(\rho) \left( \phi_1^{(n)}(\rho, \Omega) + \phi_2^{(n)}(\rho, \Omega) + \phi_3^{(n)}(\rho, \Omega) \right) \end{aligned}$$

Solve radial equations:  $f_n(\rho)$  and complex energy eigenvalues

Table 1: Components included in the three-body calculations have  $K_{max} = 20$  except those specified here. The left part refers to the components in the first Jacobi set ( $\mathbf{x}$  connecting the two nucleons), and the right part to the ones in the second and third Jacobi sets ( $\mathbf{x}$  connecting the alpha-particle and one of the nucleons).

1 <sup>st</sup> Jacobi set						2 <sup>nd</sup> and 3 <sup>rd</sup> Jacobi sets					
											
$\ell_x$	$\ell_y$	$L$	$s_x$	$s_y$	$K_{max}$	$\ell_x$	$\ell_y$	$L$	$s_x$	$s_y$	$K_{max}$
0	2	2	0	0	180	0	2	2	1/2	0	44
2	0	2	0	0	180	0	2	2	1/2	1	44
1	1	1	1	1	180	2	0	2	1/2	0	70
1	1	2	1	1	64	2	0	2	1/2	1	44
2	2	2	0	0	90	1	1	1	1/2	1	240
1	3	2	1	1	42	1	1	2	1/2	0	240
3	1	2	1	1	42	1	1	2	1/2	1	44
2	4	2	0	0	54	2	2	1	1/2	1	32
4	2	2	0	0	54	2	2	2	1/2	0	50
4	4	2	0	0	68	2	2	2	1/2	1	42
						1	3	2	1/2	0	42
						1	3	2	1/2	1	42

Notice Jacobi coordinates

Each of the Faddeev components are partial wave expanded

Rather large  $K_{max}$  in each of these many partial waves

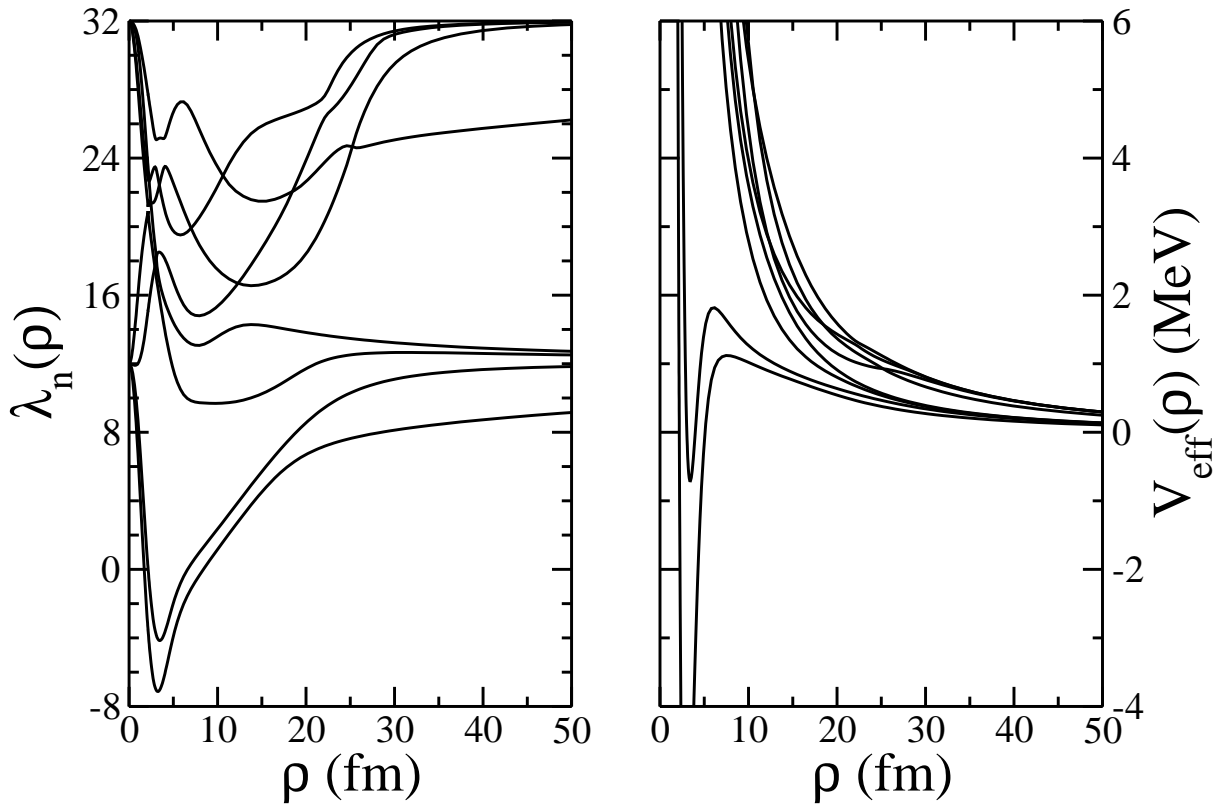


Figure 1: The real parts of the lowest 8 angular eigenvalues (left) and corresponding adiabatic potentials (right) as functions of  $\rho$  for the  $2^+$  states in  ${}^6\text{He}$  ( ${}^4\text{He} + n + n$ ). The scaling angle is  $\theta = 0.10$ .

Effective hyperradial potentials  
 Attractive region and a barrier

Resonance properties:

Energy determined by attractive pocket

Width determined by the barrier

Large-distance behavior determines final state energy distribution

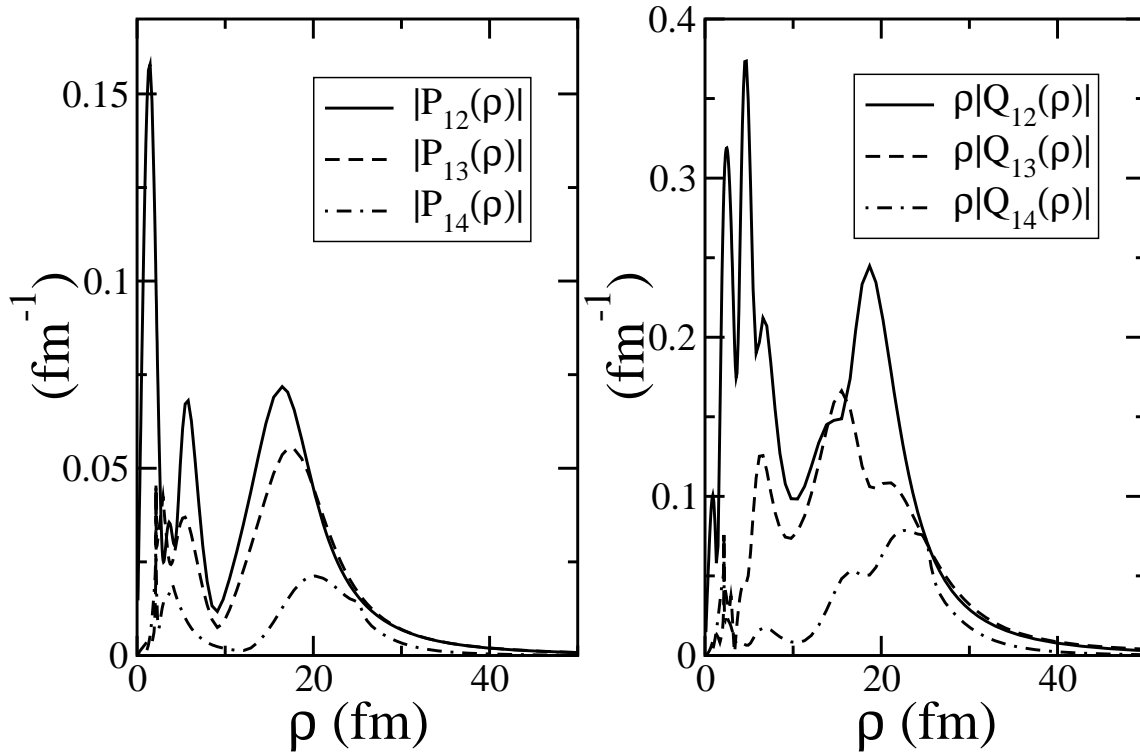


Figure 2: The coupling potentials between the four lowest adiabatic levels for  $\theta = 0.10$  shown as functions of  $\rho$  for  ${}^6\text{He}(2^+)$ . The first and the fourth levels have similar quantum numbers but approach the  $K = 2$  and 4 levels, respectively. To show the first ( $P$ ) and second ( $Q$ ) order coupling potentials in the same units ( $\text{fm}^{-1}$ ) we multiply  $Q$  by  $\rho$ . (The energy unit is restored in the coupling potentials by including the omitted factor, i.e.  $\hbar^2 Q/(2m)$ ,  $\hbar^2 P/(2m)\partial/\partial\rho$ ).

Couplings determine relative size of radial wavefunctions  
 Fall off at intermediate distance  
 Numerical stability at large distance  
 Compromise between:  
 lowest (adiabatic) state and maintaining the structure

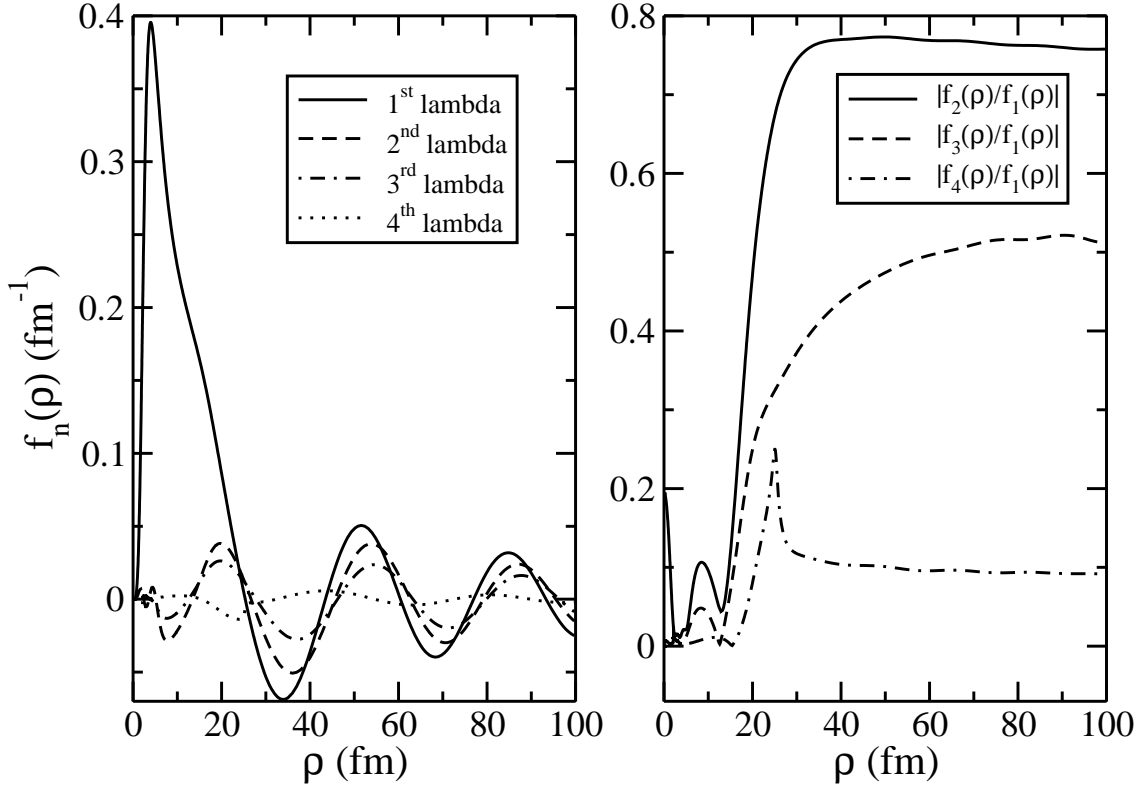


Figure 3: The lowest four radial wavefunctions (left) and their relative sizes (right) for  $\theta = 0.10$  as functions  $\rho$  for the  ${}^6\text{He}(2^+)$  resonance.

$$\Psi(\mathbf{x}, \mathbf{y}) = \sum_n f_n(\rho) \Phi_n(\rho, \Omega)$$

Each fall off exponentially while oscillating around zero  
 Relative size at large distance is stable  
 Determine energy distribution

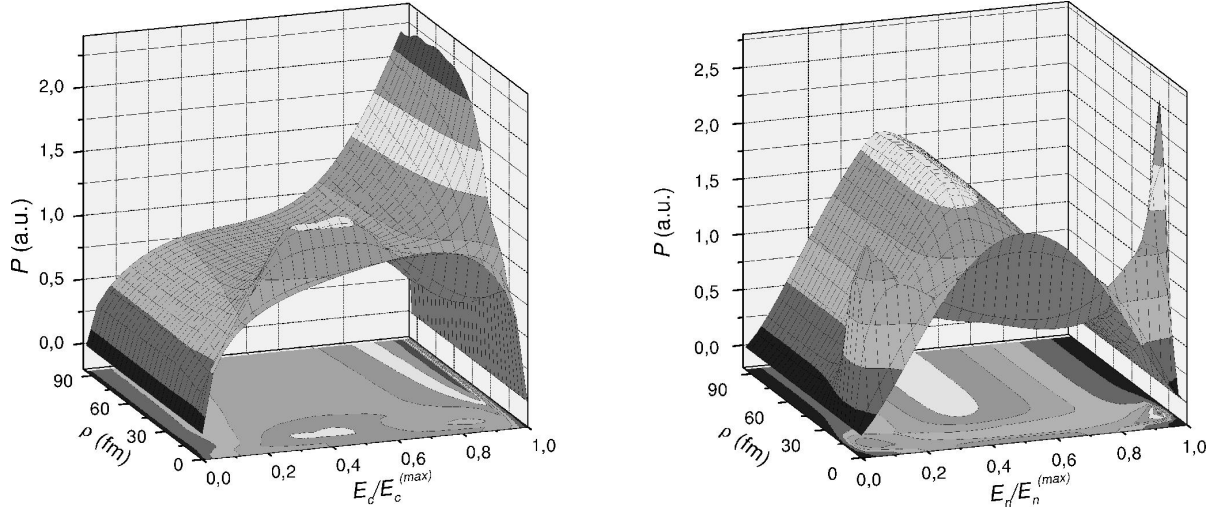


Figure 4: The energy distributions of neutrons and  $\alpha$ -particles after decay of  ${}^6\text{He}(2^+)$  for  $\theta = 0.10$ . The three-dimensional plot show the dependence on  $\rho$  with inclusion of 8 adiabatic wavefunctions. The maximum energies are  $(m_\alpha + m_n)/(m_\alpha + 2m_n)E_0$  and  $2m_n/(m_\alpha + 2m_n)E_0$  for the neutron and the  $\alpha$ -particle, respectively. Here  $E_0$  is the energy of the decaying resonance.

Kinetic energy distribution of third particle:

$$P(k_y^2) \propto P(\cos^2 \alpha) \propto \sin(2\alpha) \int d\Omega_x d\Omega_y |\Psi(\rho, \alpha, \Omega_x, \Omega_y)|^2$$

Neutrons peak at intermediate energy

$\alpha$ -particles peak at large energy

Two neutron go together, not  $\alpha$ -neutron against neutron

Virtual neutron-neutron state is essential

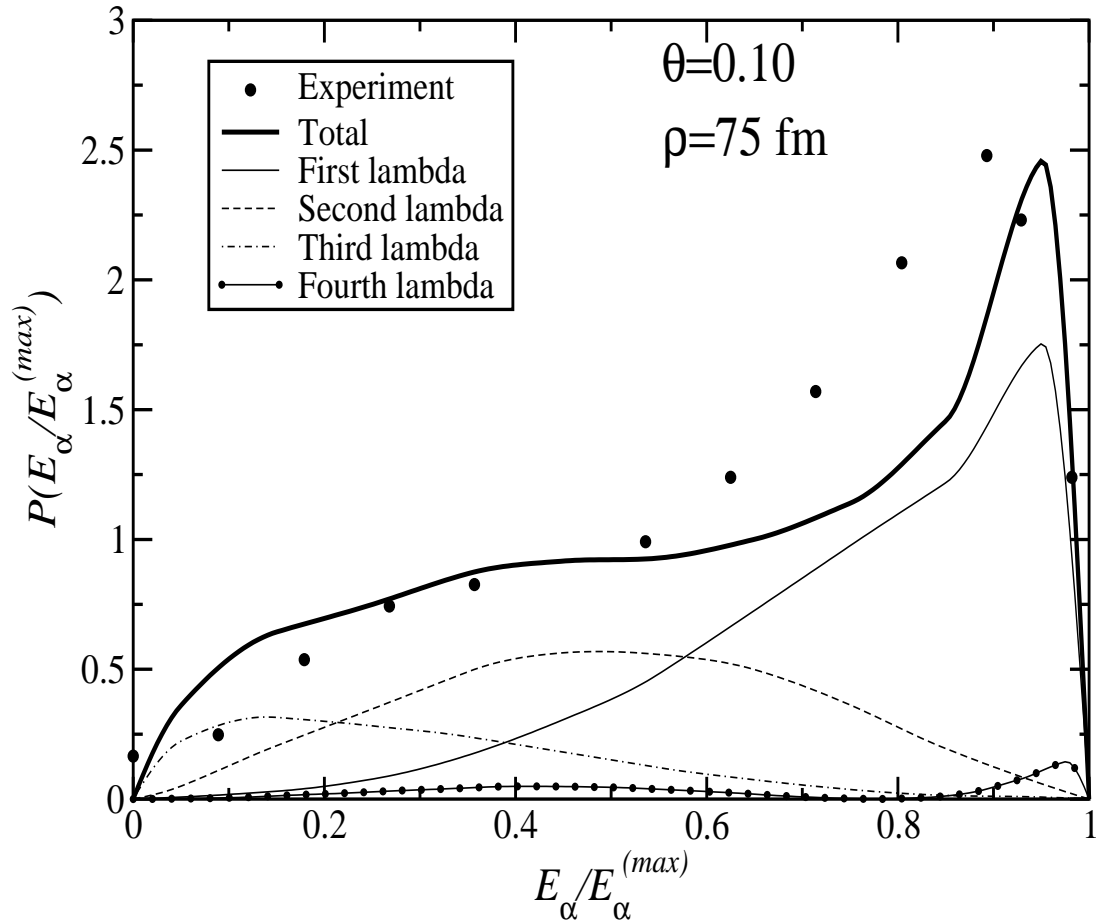


Figure 5: The energy distribution of the  $\alpha$ -particle after decay of the  $2^+$ -resonance in  ${}^6\text{He}$ . The scaling angle is  $\theta = 0.10$  and  $\rho = 75 \text{ fm}$  where convergence is reached. The points are extracted from the measurements in [10]. Contributions from the lowest 4 adiabatic potentials are shown individually.

Old data  
 Contributions from several adiabatic potentials  
 Interference is important



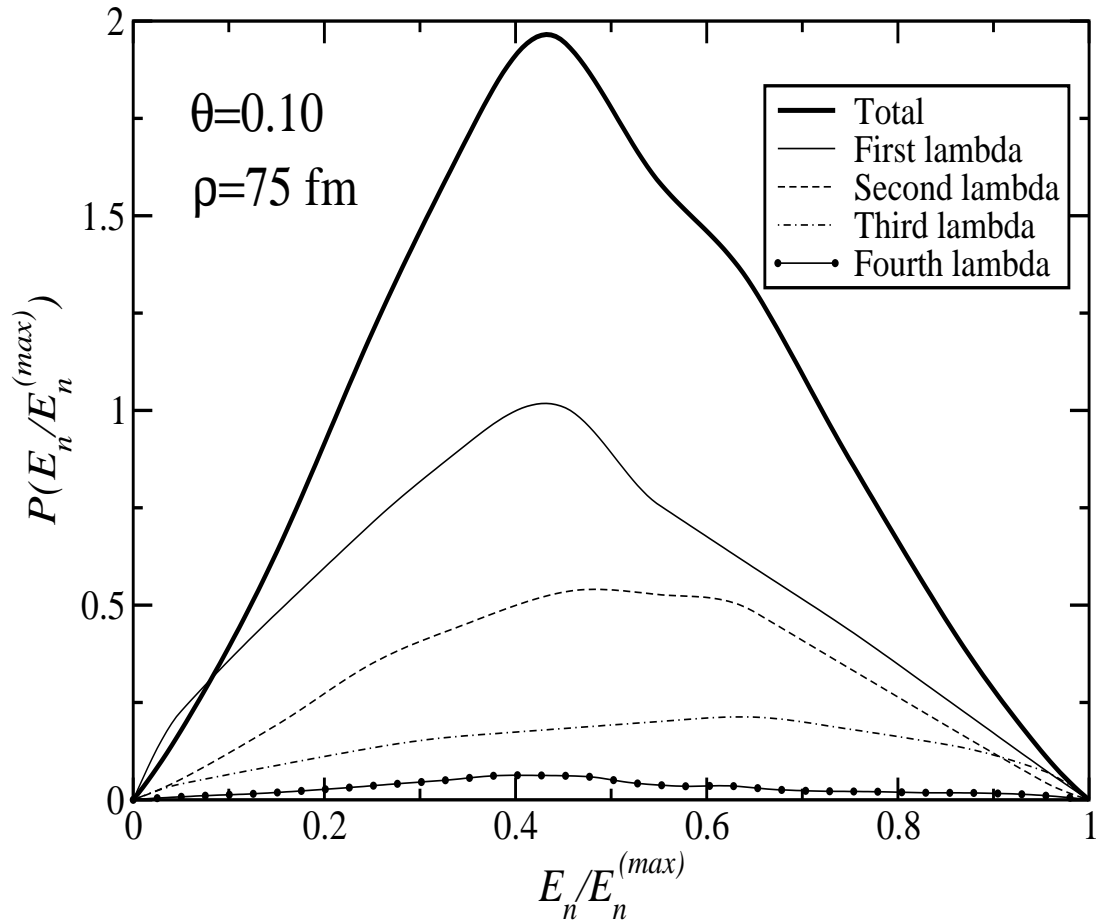


Figure 6: The energy distribution of the neutrons after decay of the  $2^+$ -resonance in  ${}^6\text{He}$ . The scaling angle is  $\theta = 0.10$  and  $\rho = 75$  fm where convergence is reached. The points are extracted from the measurements in [10]. Contributions from the lowest 4 adiabatic potentials are shown individually.

No data

Same resonance wavefunction as for  $\alpha$ -particle

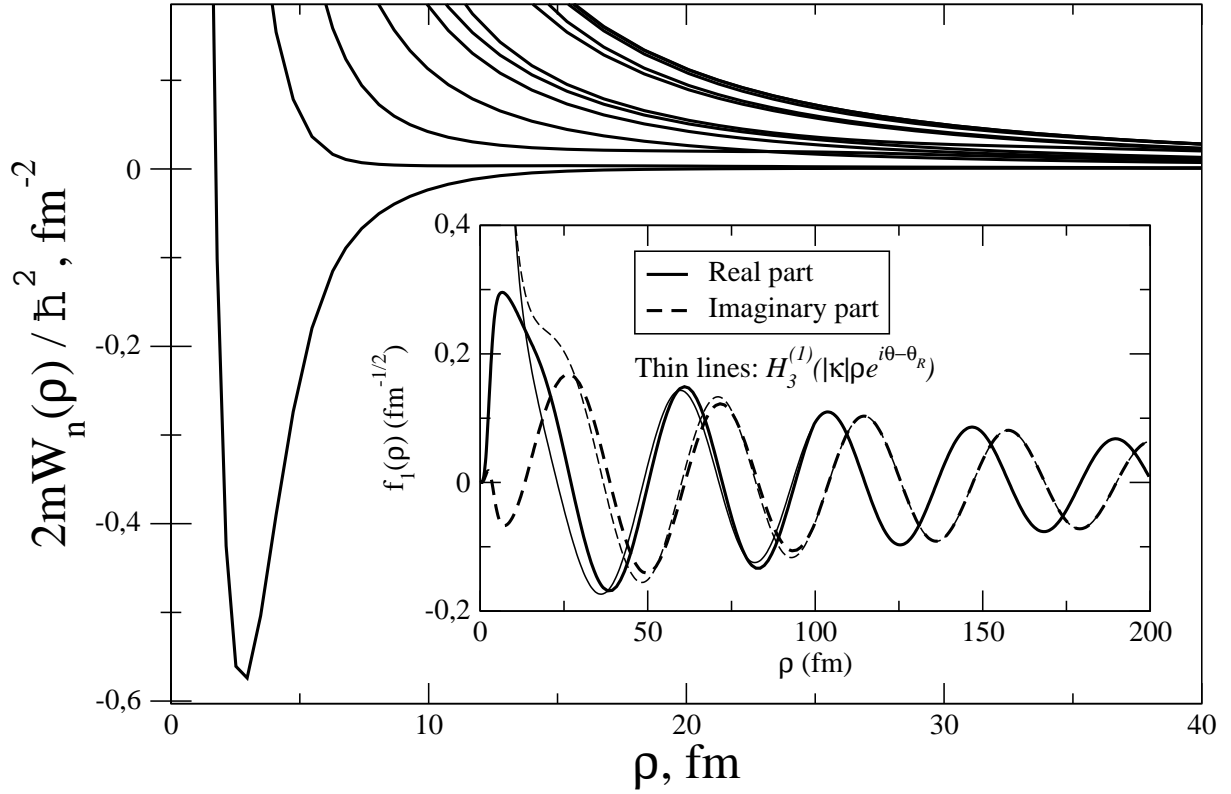


Figure 7: The lowest adiabatic potentials  $W_n(\rho)$  for the  $^{11}\text{Li}(1^-)$  halo nucleus within the three-body  $^9\text{Li}+n+n$  model with interactions from [9]. The  $n$ -core and  $n$ - $n$  scattering lengths are  $a_{nc} \approx a_{nn} \approx 20$  fm. The inset shows the lowest hyper-radial resonance function with its large distance asymptotics – the Hankel function. The complex scaling angle  $\theta = 0.15$ , the resonance angle  $\theta_R = 0.12$  corresponds to the resonance energy of about  $0.4 - 0.1i$  MeV.

Large scattering length  
Decreasing and oscillating radial function

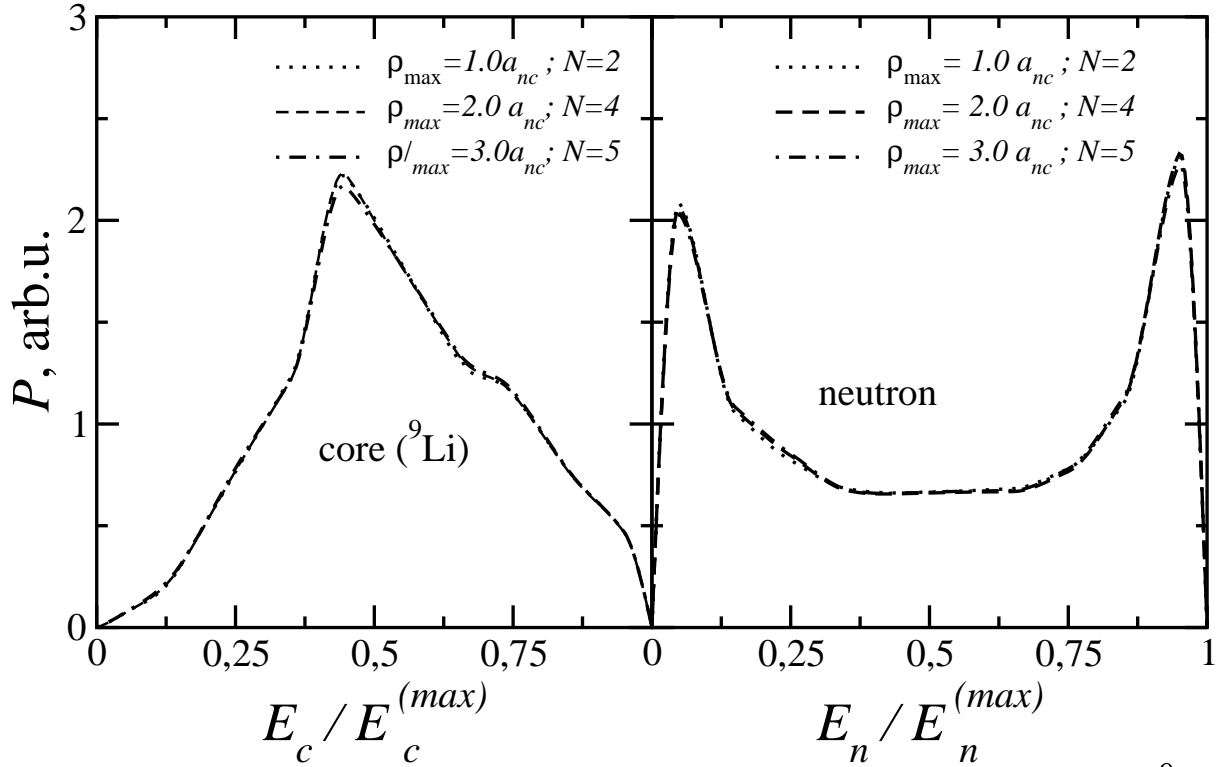


Figure 8: The energy distributions of the fragments - the core,  ${}^9\text{Li}$ , and the neutrons - in the decay of a three-body resonance  ${}^{11}\text{Li}(1^-)$  calculated in the three-body  ${}^9\text{Li} + n + n$  model with only  $s$ -wave  $n$ -core interactions (scattering length  $a_{nc} \approx 50$  fm). The different curves are calculated with different  $\rho_{max}$  and different numbers of adiabatic channels  $N$  to illustrate the convergence.

#### Schematic model

Only  $s$ -waves and large neutron-core scattering length

Lowest adiabatic function is very accurate

Very stable against large variation of  $\rho_{max}$

Core distribution peaks at intermediate energies

Neutron distribution has a low and a high energy peak

Mechanism is neutron emission, high energy

Then neutron-core stick together, low energy neutron

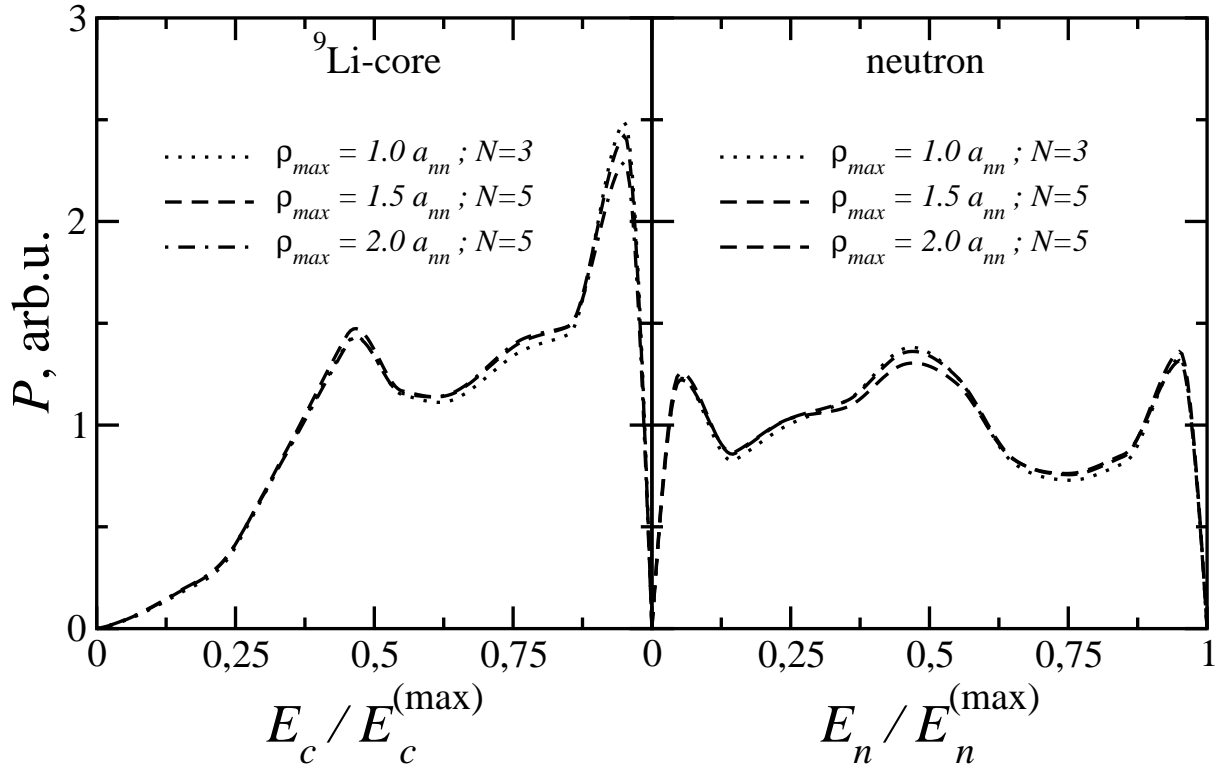


Figure 9: The energy distributions of the fragments - the core,  ${}^9\text{Li}$ , and the neutrons - in the decay of a three-body resonance  ${}^{11}\text{Li}(1^-)$  calculated in the three-body  ${}^9\text{Li} + n + n$  model with  $s$ -wave  $n$ -core interactions (scattering length  $a_{nc} \approx 50$  fm), and an  $s$ -wave interaction in the  $n - n$  subsystem (scattering length  $a_{nn} \approx a_{nc} \approx 50$  fm). The different curves are calculated with different  $\rho_{max}$  and different numbers of adiabatic channels  $N$  to illustrate the convergence.

#### Schematic model

Only  $s$ -waves, and large neutron-neutron and neutron-core scattering length

Lowest adiabatic function is very accurate

Very stable against large variation of  $\rho_{max}$

Core distribution gets new peak at high energy

Neutron distribution gets a new peak at intermediate energy

Two coherent decay mechanisms: Neutron emission, high and low energy neutrons, intermediate core energy

Core emission, two neutrons stick together

Core energy is maximum, neutron energy is intermediate

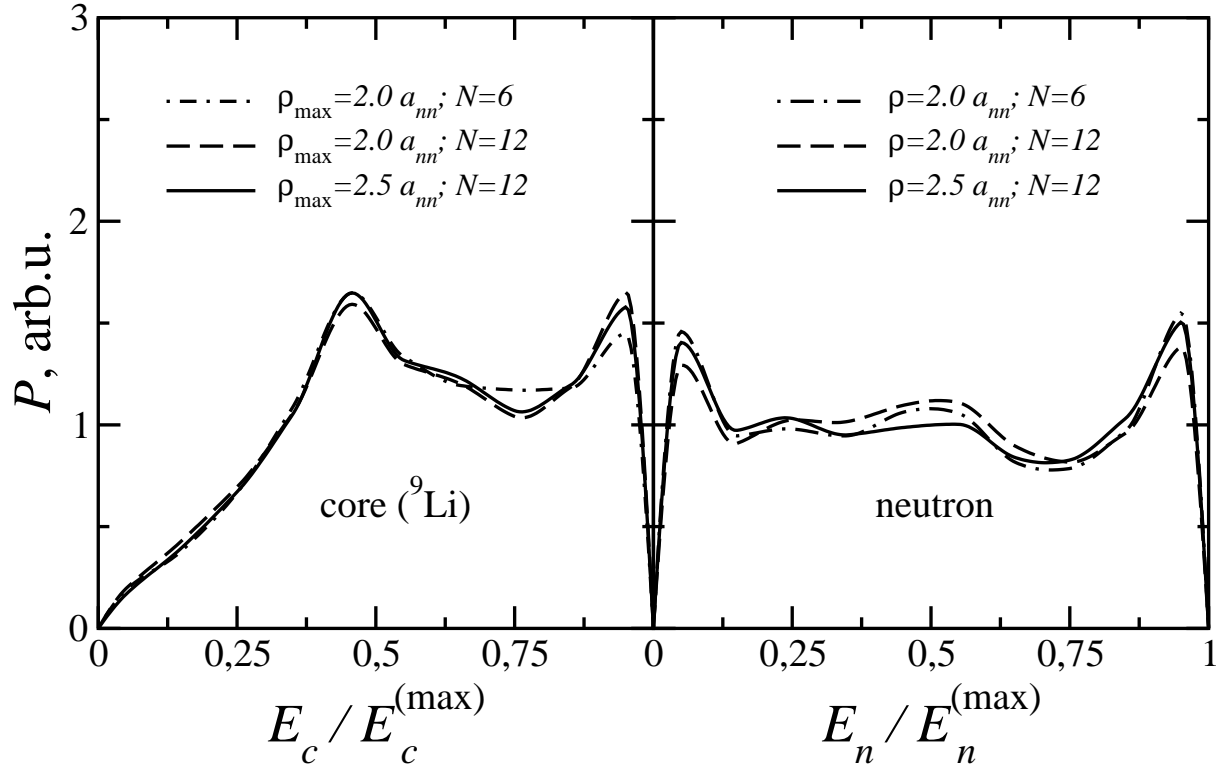


Figure 10: The energy distributions of the fragments - the core,  ${}^9\text{Li}$ , and the neutrons - in the decay of a three-body resonance  ${}^{11}\text{Li}(1^-)$  calculated with interactions from [9] where the  $n$ -core and  $n$ - $n$  scattering lengths are about 20 fm.

Realistic interactions reproducing all other known  ${}^{11}\text{Li}$  properties  
 All three scattering lengths now about 20 fm  
 All peaks from schematic model remains  
 Trace of Efimov effect

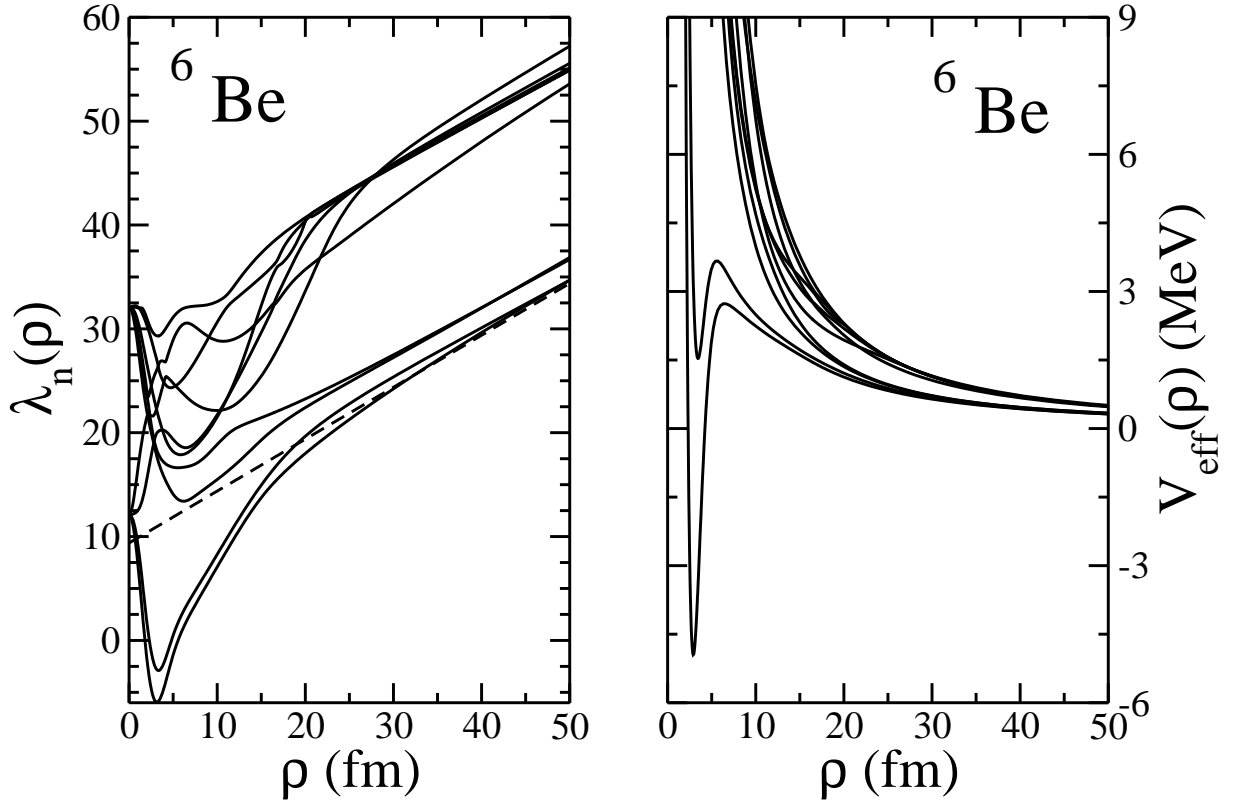


Figure 11: Real parts of the lowest 10 angular eigenvalues (left) and their corresponding adiabatic potentials (right) as functions of  $\rho$  for the  $2^+$ -resonance in  ${}^6\text{Be}$ . The scaling angle is  $\theta = 0.15$ . The dashed line is the estimated behaviour at large distances for the lowest angular eigenvalue.

The  ${}^6\text{He}$  analog  $2^+$ -resonance in  ${}^6\text{Be}$

Only difference is Coulomb

Small  $\rho$ : Same structure as for  ${}^6\text{He}$

For large  $\rho$ :

Angular eigenvalues: linear in  $\rho$ , Potentials:  $1/\rho$

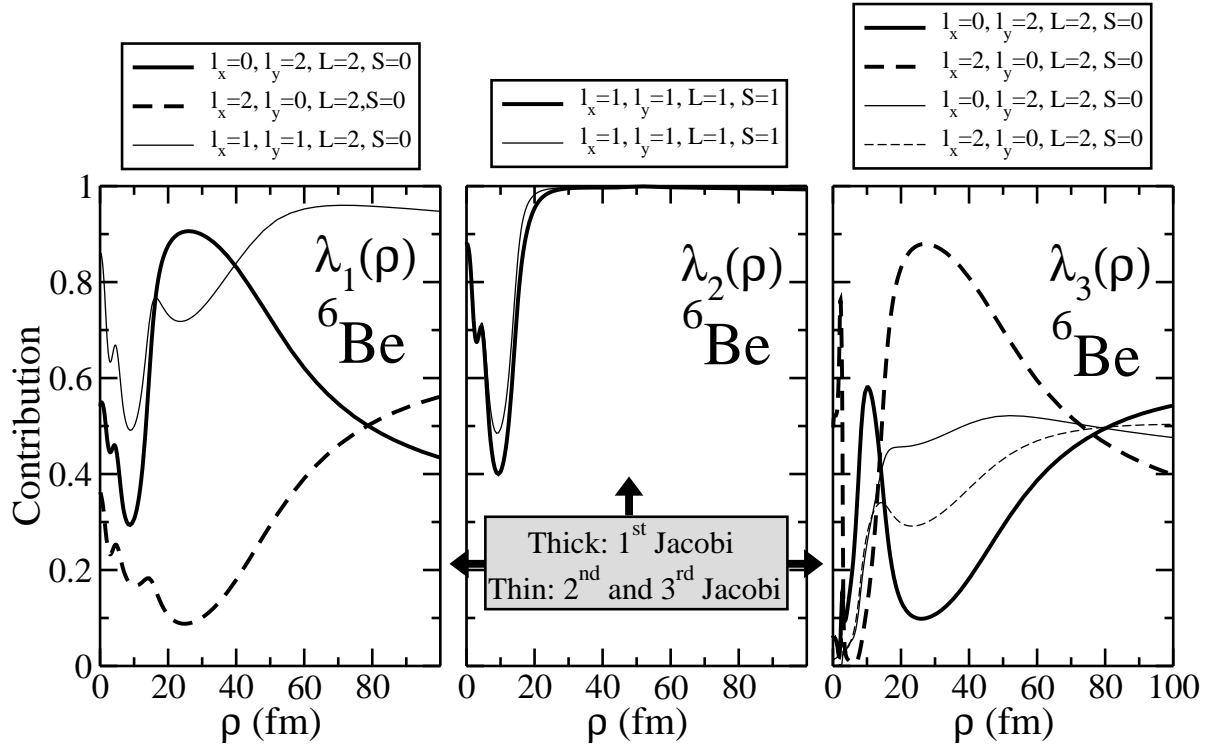


Figure 12: The fraction of the dominating components in the angular eigenfunction for the three lowest adiabatic potentials as function of  $\rho$  for  ${}^6\text{Be}$  ( $2^+$ ), see Fig. 1. The quantum numbers are as given in table 1. Thick lines:  $x$  refers to the two-proton system and  $y$  to its center of mass motion relative to the  $\alpha$ -particle. Thin lines:  $x$  refers to the proton- $\alpha$  system and  $y$  to its center of mass motion relative to the other proton.

Partial wave decomposition of angular wavefunction  
 Strong variation from small to large distance  
 First eigenvalue:  
 Proton-proton  $s$ -wave dominates at small distance  
 Proton-proton  $s$  and  $d$ -waves are comparable at large  $\rho$   
 $\alpha$ -proton  $p$ -waves dominate at large distance

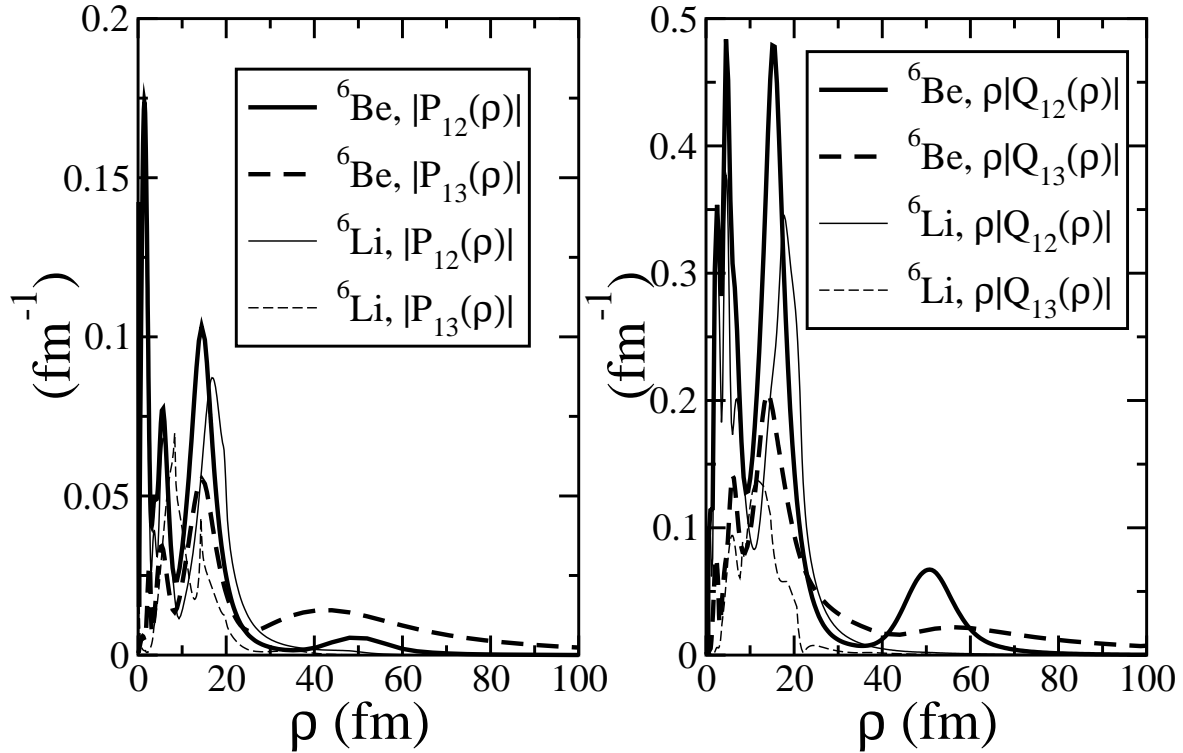


Figure 13: The absolute values of the coupling potentials between the three lowest adiabatic levels for the  $2^+$ -resonance in  ${}^6\text{Be}$  (thick curves  $\theta = 0.15$  rads) as functions of  $\rho$ , and the corresponding isobaric analog states in  ${}^6\text{Li}$  (thin curves  $\theta = 0.10$  rads).

Couplings determine relative size of radial wavefunctions  
 Fall off at intermediate distance  
 Numerical stability at large distance



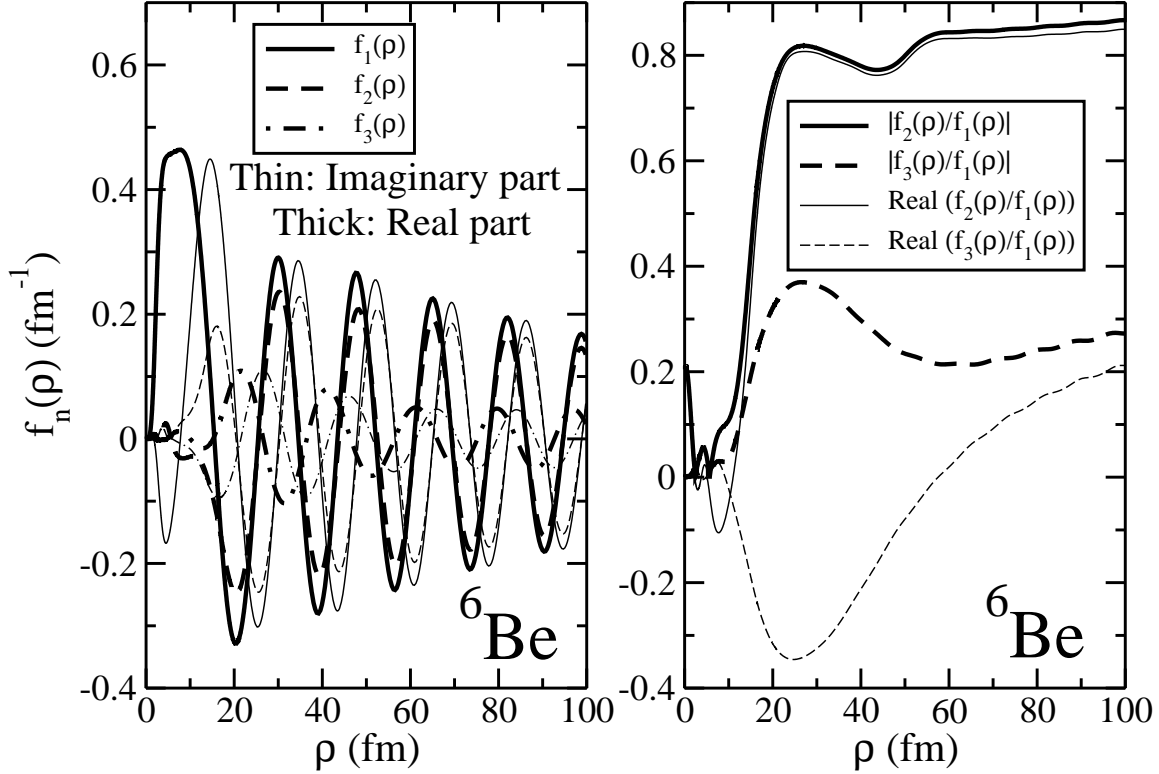


Figure 14: Left: Radial wave functions corresponding to the three first adiabatic potentials for the  $2^+$ -resonance in  ${}^6\text{Be}$ . The real and imaginary parts are shown by the thick and thin curves, respectively. Right: Absolute values (thick curves) and the real parts (thin curves) of the ratios between the radial wave functions. The probability distribution has for each  $\rho$  been normalized to 1 as function of  $\alpha$ .

$$\Psi(\mathbf{x}, \mathbf{y}) = \sum_n f_n(\rho) \Phi_n(\rho, \Omega)$$

Each fall off exponentially while oscillating around zero  
 Relative size at large distance determine energy distribution  
 Numerical stability is not obvious

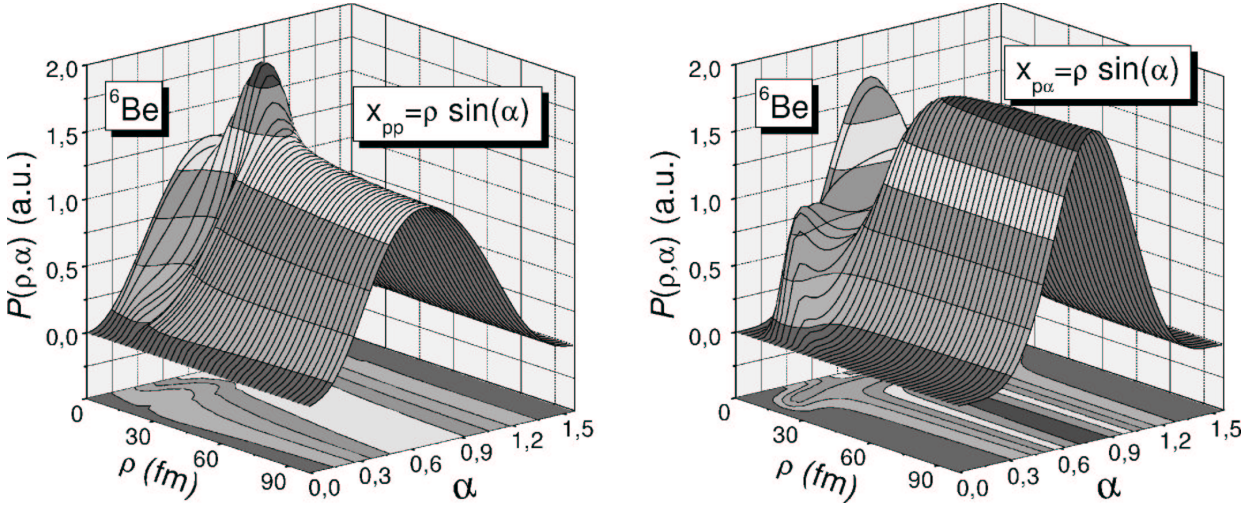


Figure 15: The probability distribution for the  $2^+$ -resonance in  ${}^6\text{Be}$  including the lowest 10 adiabatic potentials as function of the hyper-radius  $\rho$  and hyperangle  $\alpha$  related to the distance by  $r_{ik} \propto \rho \sin \alpha$ , i.e. the distance between either the one proton and core  $r_{pc}$  (right) or the two protons  $r_{pp}$  (left).

Structure of total resonance wavefunction  
 Vary strongly from small to large distance  
 Stable at larger distance  
 Much better than indicated by the first radial wavefunctions

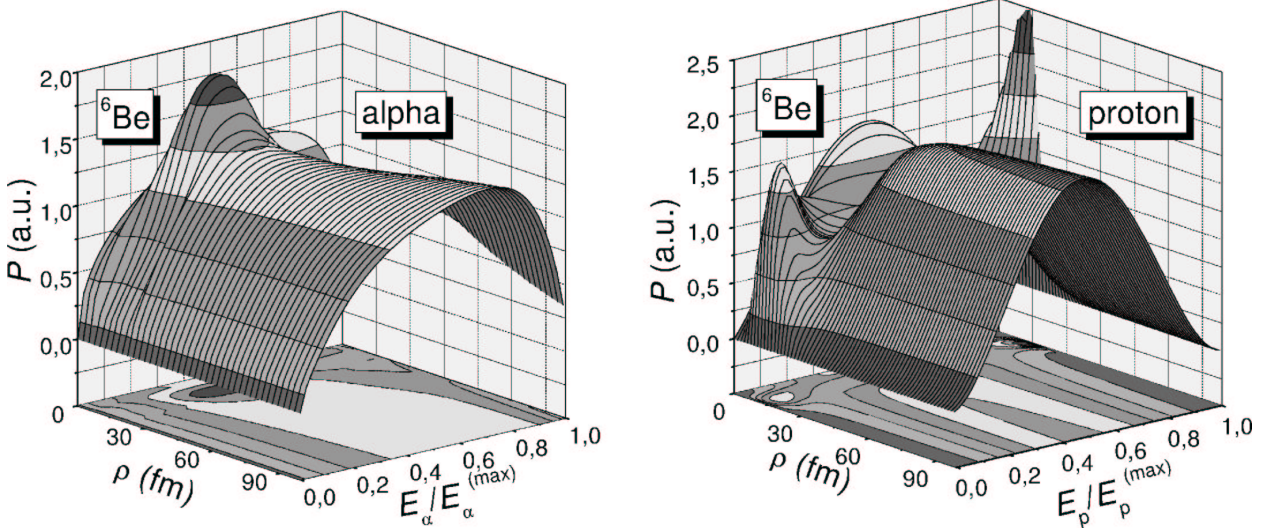


Figure 16: Kinetic energy distributions of protons (right) and  $\alpha$ -particles (left) after decay of the  $2^+$ -resonance in  ${}^6\text{Be}$ . The three-dimensional plots show the dependence on  $\rho$  with inclusion of 10 adiabatic wave functions as function of  $\cos^2 \alpha$ , i.e. the kinetic energies  $E_{\alpha,p}$  are in units of their maximum values  $E_{\alpha,p}^{(max)}$  given by  $(m_\alpha + m_p)/(m_\alpha + 2m_p)E_R$  and  $2m_p/(m_\alpha + 2m_p)E_R$  for the proton and the  $\alpha$ -particle, respectively, where  $E_R$  is the energy of the decaying resonance.

Kinetic energy distribution of third particle:

$$P(k_y^2) \propto P(\cos^2 \alpha) \propto \sin(2\alpha) \int d\Omega_x d\Omega_y |\Psi(\rho, \alpha, \Omega_x, \Omega_y)|^2$$

Protons peak at intermediate energy

$\alpha$ -particles with broad peak tilted towards large energy

Coulomb is coupling a lot and broadening distributions

Virtual proton-proton state is not present or very weak

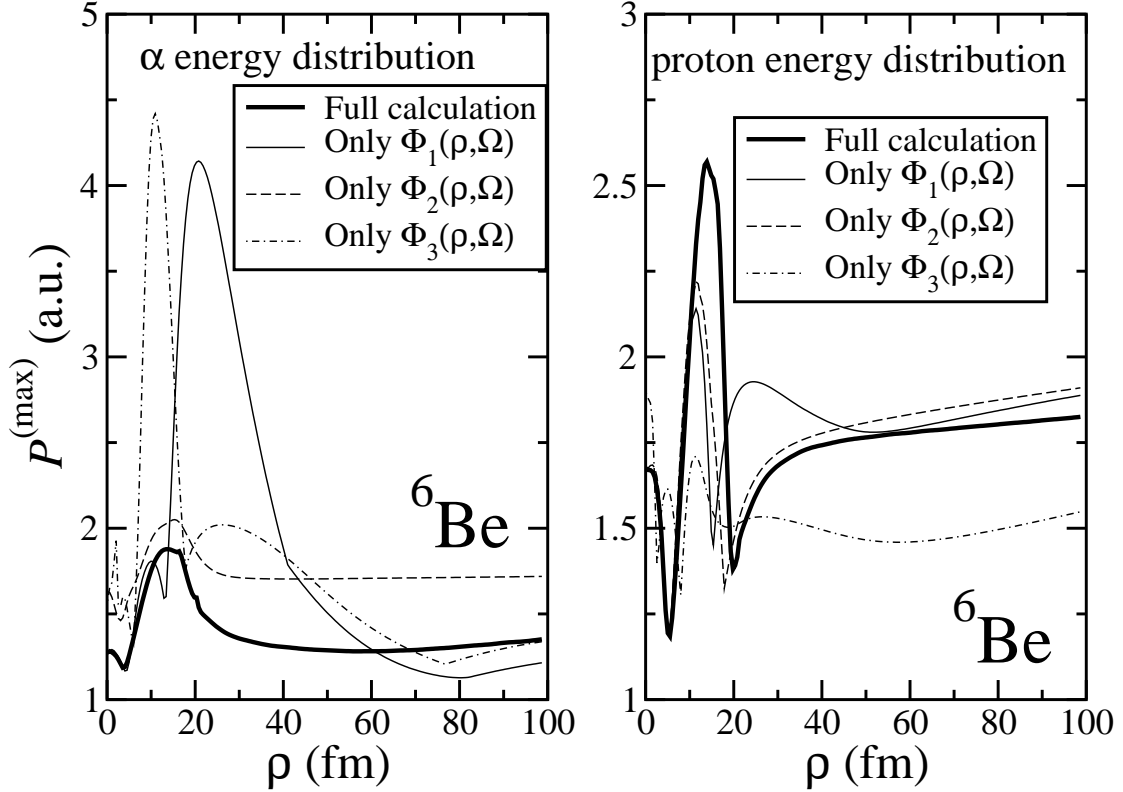


Figure 17: Projections of kinetic energy distributions for  ${}^6\text{Be}$ -decay. Thick curves: Projection of the  $\alpha$  (left panel) and proton (right panel) kinetic energy distributions (Fig. 10) on the  $E_{\alpha,p}/E_{\alpha,p}^{(max)} = 1$  plane. They are then the profile originating from the maximum values of the energy distribution for each value of  $\rho$ . The thin curves are the same profile but when respectively only the first adiabatic term (solid), only the second adiabatic term (dashed), or only the third adiabatic term (dot-dashed) is included in the calculation.

The kinetic energy distribution is redistributed with  $\rho$   
The total distribution is much more stable (thick curves)

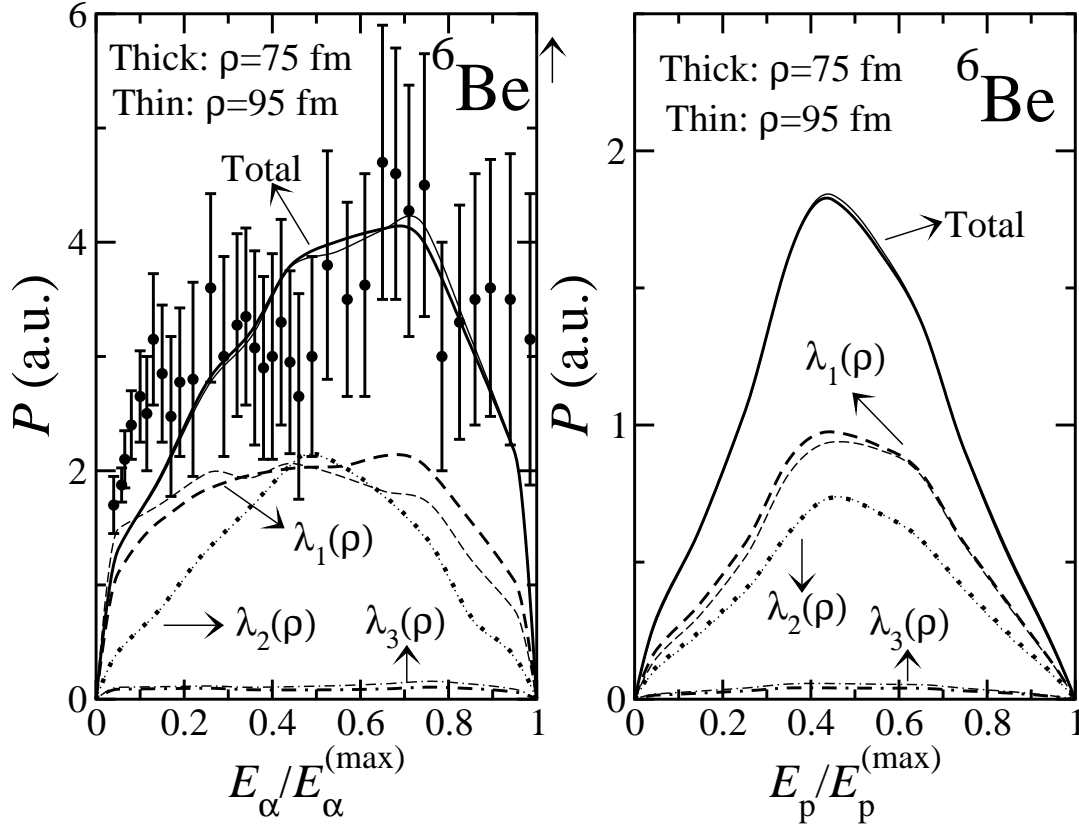


Figure 18: The kinetic energy distribution of the  $\alpha$ -particle (upper part) and the proton (lower part) after decay of the  $2^+$ -resonance in  ${}^6\text{Be}$ . The scaling angle is  $\theta = 0.15$  and the two sets of curves are for  $\rho = 75, 95$  fm. The points are extracted from the measurements in [10]. Contributions from the lowest adiabatic potentials are shown individually.

Old data for  $\alpha$ -particle  
 Contributions from several adiabatic potentials

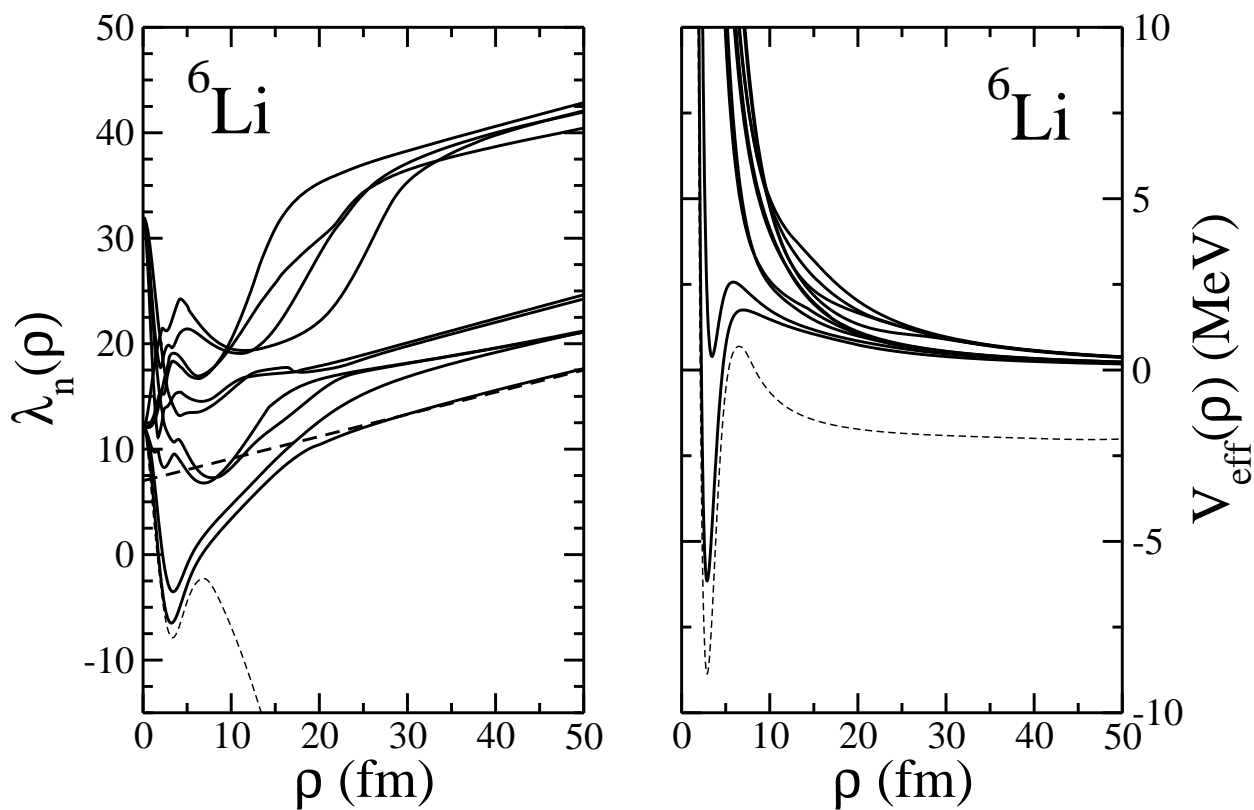


Figure 19: Real parts of the lowest 10 angular eigenvalues (left) and their corresponding adiabatic potentials (right) as functions of  $\rho$  for the  $2^+$ -resonance in  ${}^6\text{Li}$ . The scaling angle is  $\theta = 0.10$ . The dashed line is the estimated behaviour at large distances for the lowest angular eigenvalue.

The  ${}^6\text{He}$  analog  $2^+$ -resonance in  ${}^6\text{Li}$

Only difference is Coulomb

Small  $\rho$ : Same structure as for  ${}^6\text{He}$

For large  $\rho$ :

Angular eigenvalues: linear in  $\rho$ , Potentials:  $1/\rho$

One more state:

$\alpha$ -deuteron structure, eigenvalue as  $-\rho^2$ , potential to constant

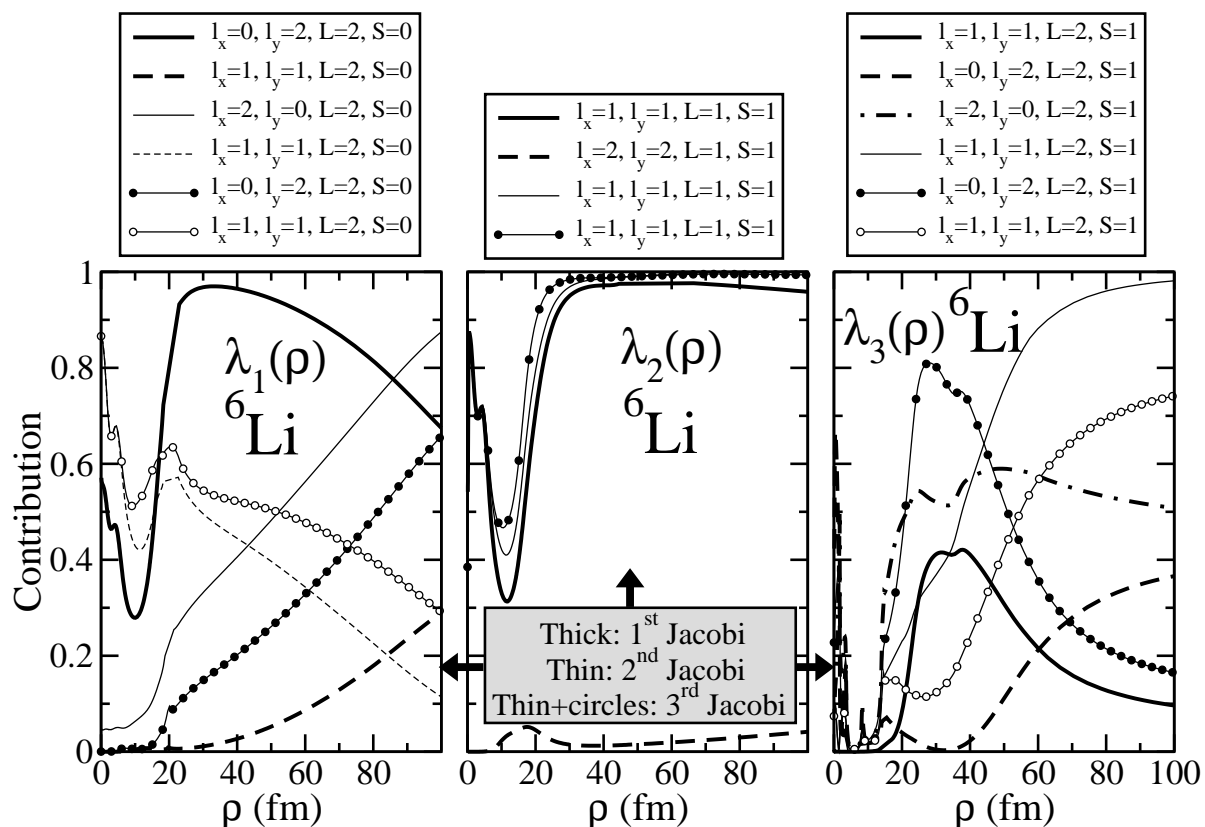


Figure 20: The fraction of the dominating components in the angular eigenfunction for the three lowest adiabatic potentials as function of  $\rho$  for  ${}^6\text{Li}$  ( $2^+$ ). The quantum numbers are as given in table 1. We omitted the almost decoupled lowest eigenfunction of deuteron- $\alpha$  character. In the second Jacobi set (thin lines) the  $x$  refers to the proton- $\alpha$  system and  $y$  to its center of mass motion relative to the neutron. In the third Jacobi set (thin+circle lines) the  $x$  refers to the neutron- $\alpha$  system and  $y$  to its center of mass motion relative to the proton.

Partial wave decomposition of angular wavefunction

Strong variation from small to large distance

First eigenvalue:

Proton-proton s-wave vary but dominates at all distances

Proton-proton  $p$ -wave increases with  $\rho$ , isospin 0 increase with  $\rho$

$\alpha$ -proton  $d$ -wave dominates at large distance

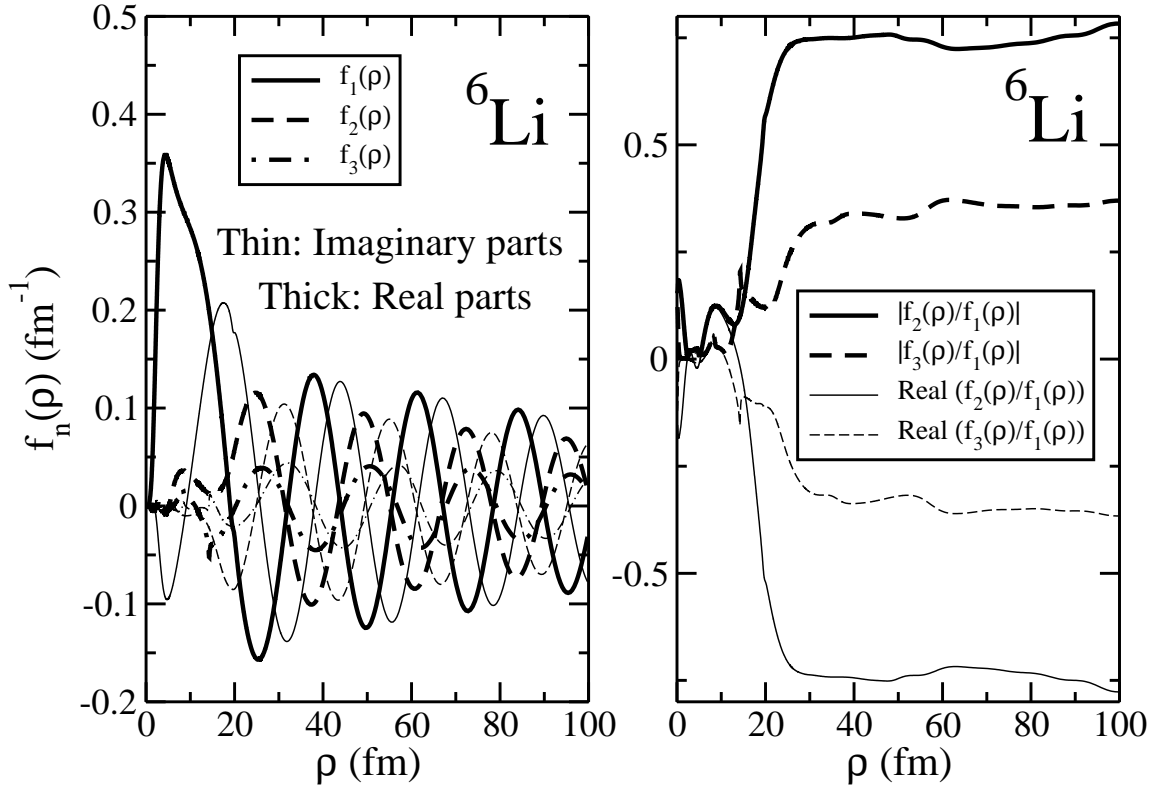


Figure 21: Left: Radial wave functions corresponding to the three first adiabatic potentials for the  $2^+$ -resonance in  ${}^6\text{Li}$ . The real and imaginary parts are shown by the thick and thin curves, respectively. Right: Absolute values (thick curves) and the real parts (thin curves) of the ratios between the radial wave functions. The probability distribution has for each  $\rho$  been normalized to 1 as function of  $\alpha$ .

Each fall off exponentially while oscillating around zero  
 Relative size at large distance determine energy distribution  
 Numerical stability is established



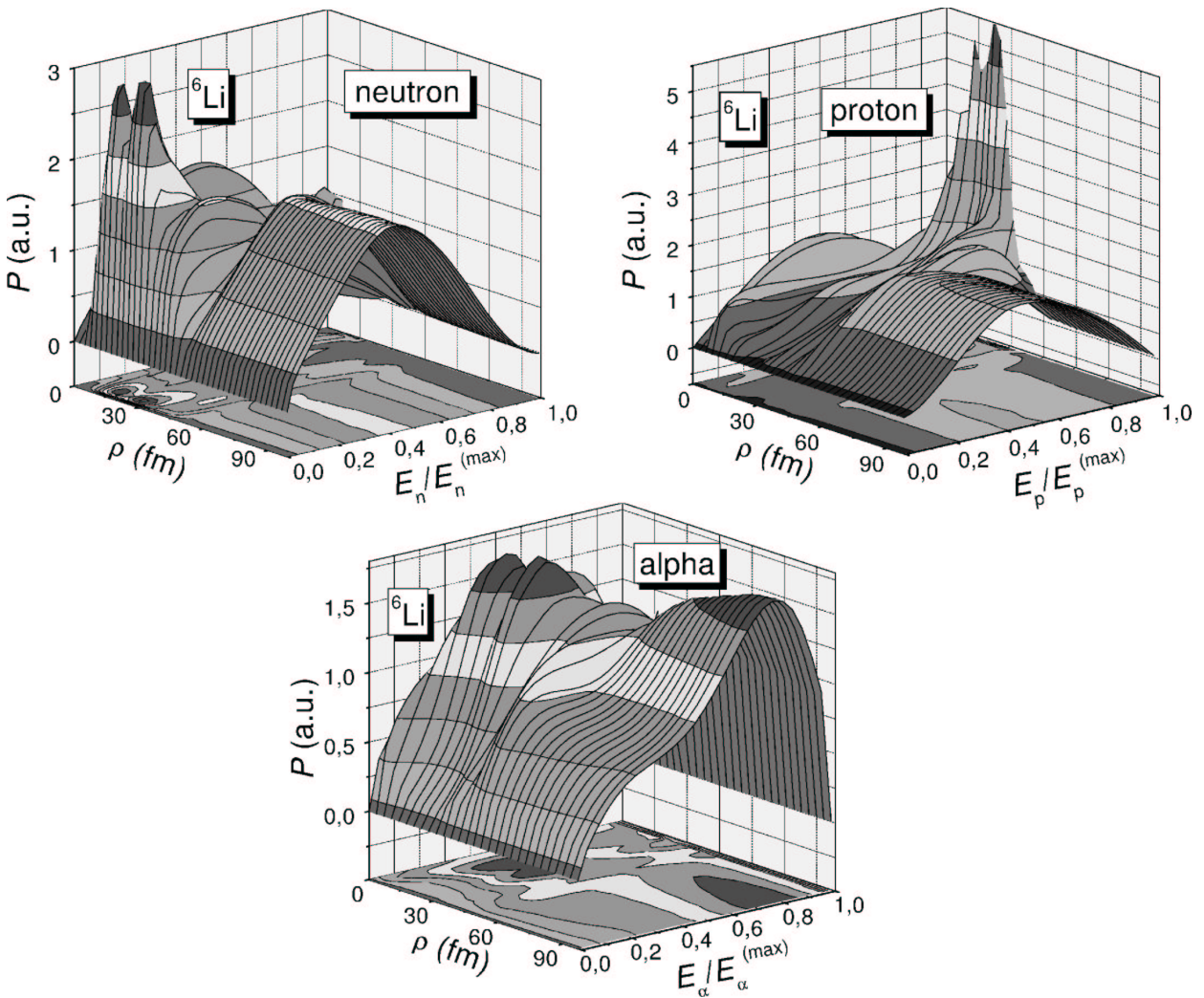


Figure 22: Kinetic energy distributions of protons (upper-right panel), neutrons (upper-left panel), and  $\alpha$ -particles (lower panel) after decay of the  $2^+$ -resonance in  ${}^6\text{Li}$  corresponding to that of Fig. 10. The three-dimensional plot show the dependence on  $\rho$  with inclusion of 10 adiabatic wave functions. The maximum energies  $E_{n,p,\alpha}^{(max)}$  are  $(m_\alpha + m_p)/(m_\alpha + m_n + m_p)E_R$ ,  $(m_\alpha + m_n)/(m_\alpha + m_n + m_p)E_R$  and  $(m_n + m_p)/(m_\alpha + m_n + m_p)E_R$  for the neutron, the proton, and the  $\alpha$ -particle, respectively, where  $E_R$  is the energy of the decaying resonance.

Kinetic energy distribution of third particle:

$$P(k_y^2) \propto P(\cos^2 \alpha) \propto \sin(2\alpha) \int d\Omega_x d\Omega_y |\Psi(\rho, \alpha, \Omega_x, \Omega_y)|^2$$

Protons peak at intermediate (higher) energy

Neutrons peak at intermediate (lower) energy

$\alpha$ -particles with broad peak towards large energy

Neutron and proton tend to go together

Virtual neutron-proton state is active

Coulomb is broadening distributions

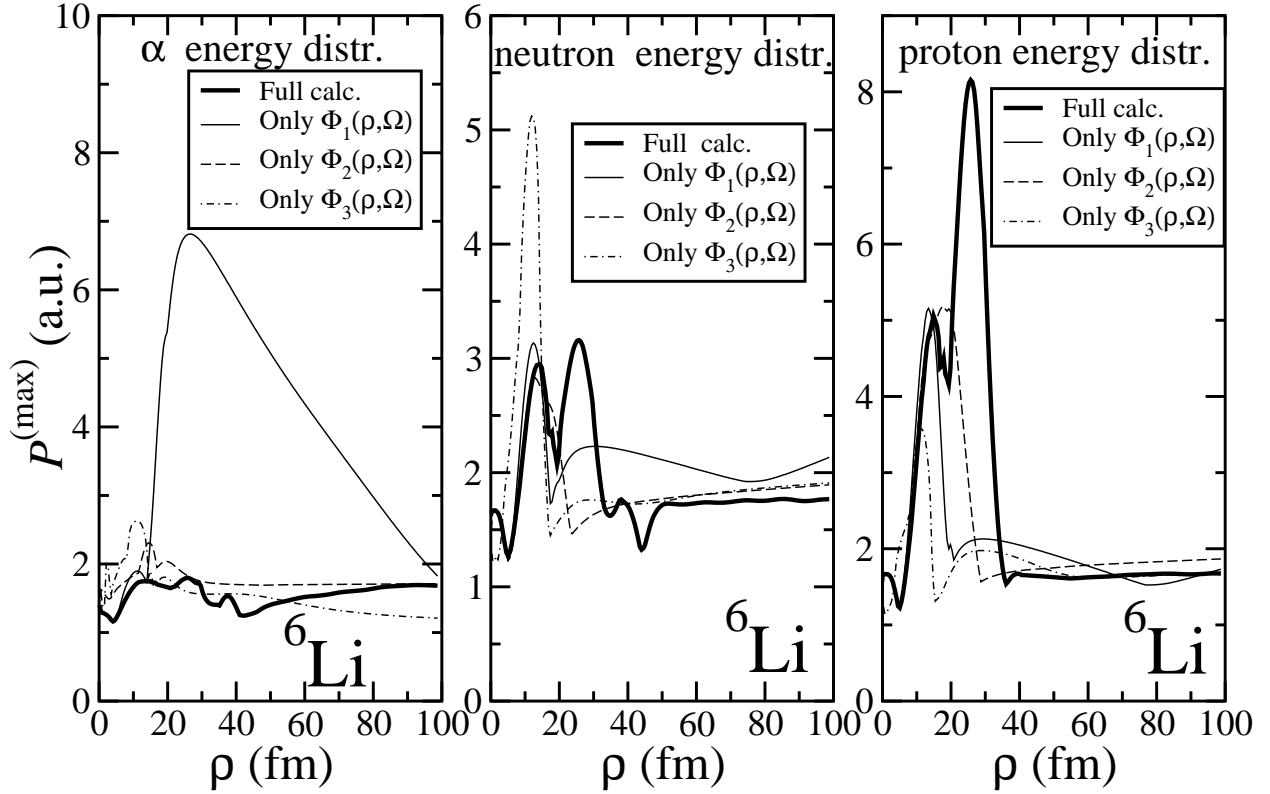


Figure 23: Projections of kinetic energy distributions as functions of  $\rho$  for  ${}^6\text{Li}(2^+)$ . Thick curves: Projection of the  $\alpha$  (left panel) and proton (right panel) kinetic energy distributions (Fig. 10) on the  $E_{\alpha,p}/E_{\alpha,p}^{(max)} = 1$  plane. They are then the profile originated by the maximum values of the energy distribution for each value of  $\rho$ . The thin curves are the same profile but when only the first adiabatic term (solid), only the second adiabatic term (dashed), or only the third adiabatic term (dot-dashed) is included in the calculation.

The kinetic energy distribution is redistributed with  $\rho$   
The total distribution is much more stable (thick curves)

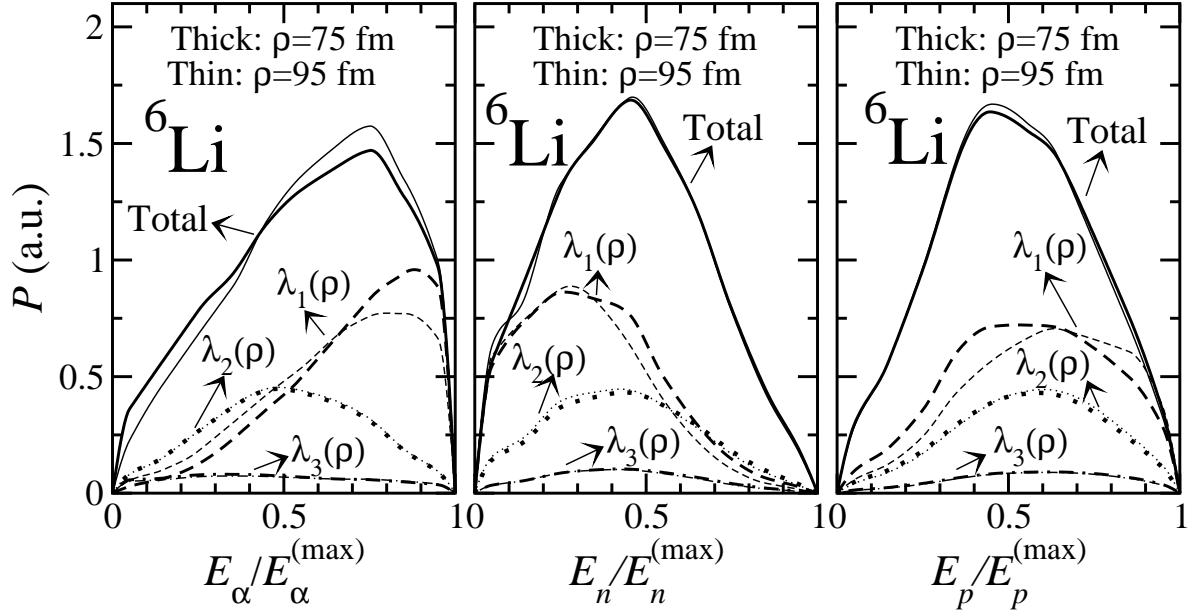


Figure 24: The kinetic energy distribution of the  $\alpha$ -particle (upper part), the neutron (middle part) and the proton (lower part) after decay of the isobaric analog  $2^+$ -resonance in  ${}^6\text{Li}$ . The scaling angle is  $\theta = 0.10$  and the two sets of curves are for  $\rho = 75, 95$  fm. The points are extracted from the measurements in [10]. Contributions from the lowest adiabatic potentials are shown individually.

Old data for  $\alpha$ -particle exist in another frame  
 Contributions from several adiabatic components  
 Protons peak at intermediate (higher) energy  
 Neutrons peak at intermediate (lower) energy  
 $\alpha$ -particles with broad peak towards large energy  
 Neutron and proton tend to go together  
 Virtual neutron-proton state is active  
 Coulomb is broadening the distributions

## CONCLUSIONS

1. Three-body decay of many-body resonances
2. A model working in practice
3. Energies must be artificially adjusted as in  $\alpha$ -decay
4. Width is estimated as hyperspherical barrier penetrability
5. Asymptotic wavefunction behavior determines the final state energy distributions
6. Asymptotics are established at intermediate distances where basis size is manageable
7. Large scattering lengths can be handled, Efimov effect
8. Coulomb can be handled in cases investigated
9. Isospin mixing is a dynamic effect occurring outside the range of short-range interactions
10. High precision, complete kinematics, high intensity,

**RIA**

## DIFFERENCES TO GRIGORENKO ET AL

1. The spin dependence of the proton-core interaction in  $^{17}\text{Ne}$  computations is in conflict with the mean-field spin-orbit interaction, i.e. the valence  $d_{3/2}$  and  $d_{5/2}$  states can not be independently populated, only specific combinations. Maybe corrected later on.

2. The hyperspherical method with only one Faddeev component is used, i.e. it is not possible to describe (i) Efimov effect, (ii) close to Efimov structure, (iii) two simultaneous 2-body substructures, (iv) one 2-body resonance unless, as he sometimes does, allow this structure as a variational degree of freedom.

3. The hyperspherical method has rather small  $Kmax \simeq 20-25$ . With three Faddeev components we need at least  $Kmax \simeq 100-150$  with only the short range interaction. The Coulomb interaction and the unavoidable couplings at large distances probably increase the necessary basis size.

4. The three-body interaction is  $\rho^{-3}$  at large distance, i.e. exactly of the same form as the effective hyperradial potentials. This should not be necessary if the proper components are accurately included. Instead this interaction should be of much shorter range in a three-body coordinate, e.g. exponential or Gaussian.

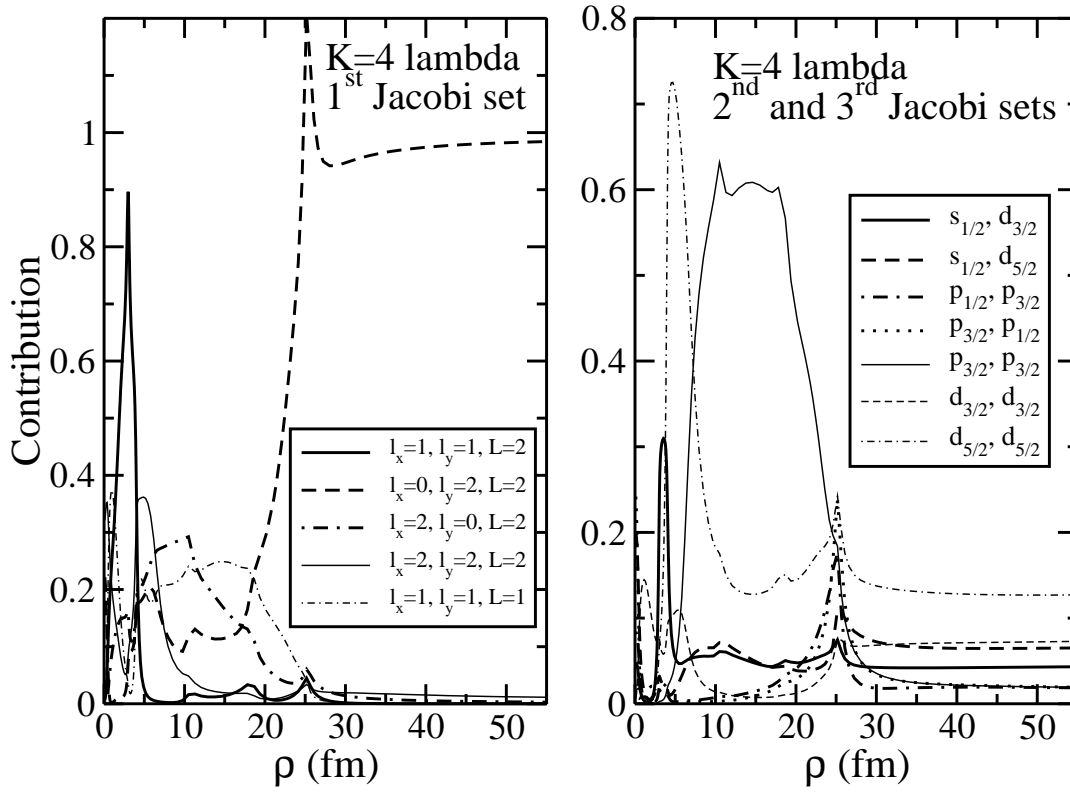


Figure 25: The fraction of different components in the fifth adiabatic potential for  $\theta = 0.10$  as function of  $\rho$  for  ${}^6\text{He}(2^+)$ . The angular eigenvalue corresponds to  $K = 4$  at large  $\rho$ , see Fig. 1. The angular momenta are specified by  $\ell_x, j_x, \ell_y, j_y$ , and  $L$ . Left:  $x$  refers to the two-neutron system and  $y$  to its center of mass motion relative to the  $\alpha$ -particle. Right:  $x$  refers to the neutron- $\alpha$  system and  $y$  to its center of mass motion relative to the other neutron. We give the  $(x, y)$  components on the figure as  $\ell_j$ .

Partial wave decomposition of angular wavefunction

Huge variation from small to large distance

Neutron-neutron s-wave dominates at large, not at small, distance

$\alpha$ -neutron  $p_{3/2}$  at small distance

All  $\alpha$ -neutron  $p$ -waves at large distance

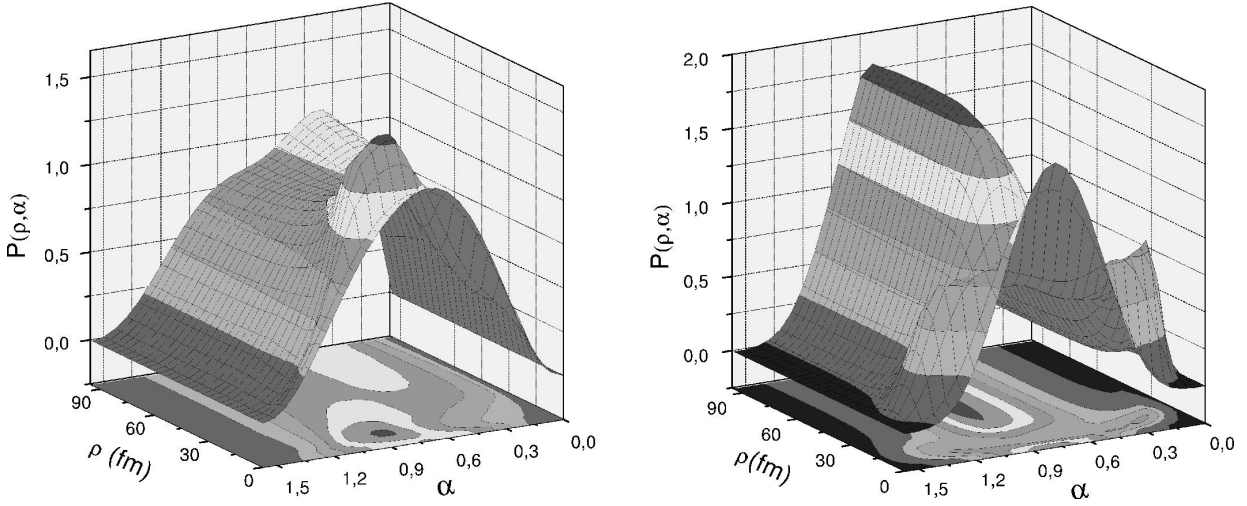


Figure 26: The probability distribution for  ${}^6\text{He}(2^+)$  including the lowest 8 adiabatic potentials as function of hyperradius  $\rho$  and hyperangle  $\alpha$  related to the distance by  $r_{ik} \propto \rho \sin \alpha$ , i.e. the distance between either the one neutron and core  $r_{nc}$  (left) or the two neutrons  $r_{nn}$  (right).

Structure of total resonance wavefunction  
 Vary strongly with distance  
 Stable at larger distance

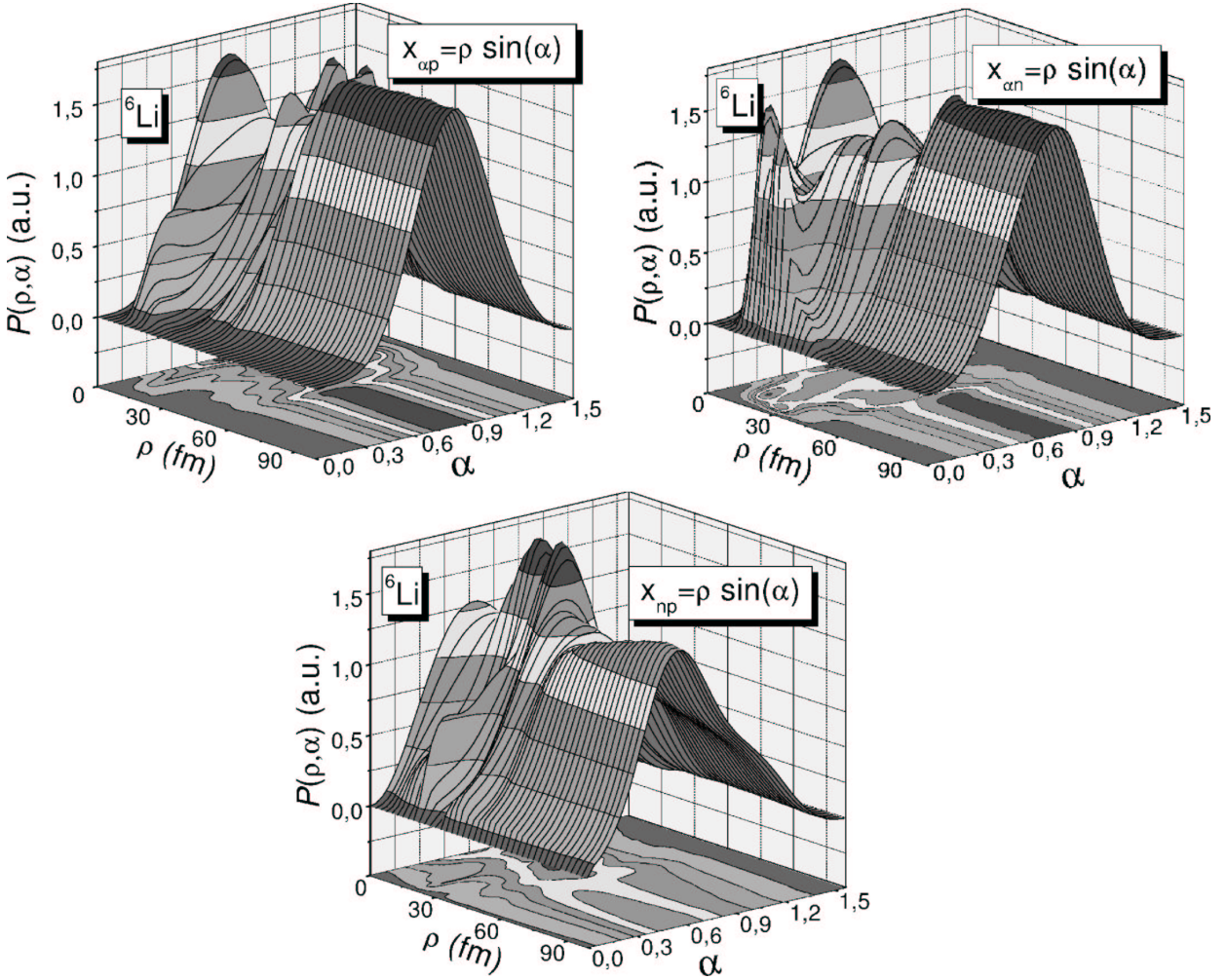


Figure 27: The probability distribution for the  $2^+$ -resonance in  ${}^6\text{Li}$  including the lowest 10 adiabatic potentials as function of the hyper-radius  $\rho$  and hyperangle  $\alpha$  related to the distance by  $r_{ik} \propto \rho \sin \alpha$ , i.e. the distance  $r_{cp}$  refers to core-proton distance in the upper-left part,  $r_{cn}$  core-neutron distance in the upper-right part, and to the  $r_{pn}$  proton-neutron distance in the lower part.

Structure of total resonance wavefunction  
 Vary strongly from small to large distance  
 Stable at larger distance



## References

- [1] E. Nielsen, D.V. Fedorov, A.S. Jensen and E. Garrido, The three-body problem with short-range interactions, *Phys. Rep.* **347**, 373-459 (2001).
- [2] A.S. Jensen, K. Riisager, D.V. Fedorov and E. Garrido, Structure and reactions of quantum halos, *Rev. Mod. Phys.* **76** (2004) 215-261.
- [3] E. Garrido, D.V. Fedorov, and A.S. Jensen, Origin of three-body resonances, *Eur. Phys. J.* **A25** (2005) 365.
- [4] E. Garrido, D.V. Fedorov, A.S. Jensen and H.O.U. Fynbo, Anatomy of three-body decay. I. Schematic models, *Nucl. Phys.* **A748** (2005) 27.
- [5] E. Garrido, D.V. Fedorov, A.S. Jensen and H.O.U. Fynbo, Anatomy of three-body decay. II. Decay mechanism and resonance structure, *Nucl. Phys.* **A748** (2005) 39.
- [6] E. Garrido, D.V. Fedorov, A.S. Jensen and H.O.U. Fynbo, Anatomy of three-body decay. III. Energy distributions, *Nucl. Phys.* **A766** (2006) 74.
- [7] E. Garrido, D.V. Fedorov, H.O.U. Fynbo, and A.S. Jensen, Energy distributions of charged particles from three-body decay, Submitted for publication.

- [8] E. Garrido, D.V. Fedorov and A.S. Jensen,  
Efimov effect in nuclear three-body resonance decays,  
Phys. Rev. Lett. , (2006), in press.
- [9] E. Garrido, D.V. Fedorov and A.S. Jensen, Nucl. Phys. **A708**,  
277 (2002).
- [10] B.V. Danilin, M.V. Zhukov, A.A. Korshennikov, L.V.  
Chulkov, V.D. Efros, Sov. J. Nucl. Phys. **46** (1987) 225.